Lab on a Chip

RSC Publishing

PAPER

An intelligent digital microfluidic system with fuzzy-enhanced feedback for multi-droplet manipulation†

Cite this: *Lab Chip*, 2013, **13**, 443

Jie Gao,‡[a] Xianming Liu,‡[b] Tianlan Chen,[a] Pui-In Mak,[a] Yuguang Du,[b] Mang-I Vai,[a] Bingcheng Lin*[b] and Rui P. Martins*[ac]

Received 19th October 2012,
Accepted 27th November 2012

DOI: 10.1039/c2lc41156c

www.rsc.org/loc

The complexity of droplet hydrodynamics on a digital microfluidic (DMF) system eventually weakens its potential for application in large-scale chemical/biological micro-reactors. We describe here an intelligent DMF technology to address that intricacy. A wide variety of control-engaged droplet manageability is proposed and demonstrated through the operation of our modular DMF prototype, which comprises: (*i*) rigid profiling ability of different droplet's hydrodynamics under a real-time trajectory track of droplet-derived capacitance, permitting accurate and autonomous multi-droplet positioning without visual setup and heavy image signal processing; (*ii*) fuzzy-enhanced controllability saving up to 21% charging time when compared with the classical approach, enhancing the throughput, fidelity and lifetime of the DMF chip, while identifying and renouncing those weakened electrodes deteriorated over time, and (*iii*) expert manipulability of multi-droplet routings under countermeasure decisions in real time, preventing droplet-to-droplet or task-to-task interference. Altogether, this work exhibits the first modular DMF system with built-in electronic-control software-defined intelligence to enhance the fidelity and reliability of each droplet operation, allowing future manufacturability of a wide range of life science analyses and combinatorial chemical screening applications.

1 Introduction

The manageable electrowetting-on-dielectric (EWOD) behavior of microdroplets, under variable-charged surface electrodes, has inspired the development of digital microfluidic (DMF) systems for large-scale micro-reactors,[1,2] which have underpinned a wide variety of chemical or biological applications in tiny droplet volumes such as molecular probe synthesis,[3,4] proteomics,[5] immunoassays,[6] enzyme assays,[7] clinical diagnostics,[8] DNA sample processing[9] and cell-based assays.[10,11]

DMF belongs to a class of two-dimensional plane or curved-geometry[12] electronic control systems with the electrodes coated with dielectric and hydrophobic materials. The manipulation of a droplet is achieved *via* surface-tension modulation induced by an electric field. Their open structure (*i.e.*, no preset microchannel), scalability and high compatibility with diverse aqueous, organic[13] or ionic liquids,[14] beneficially position them ahead of traditional channel microfluidics,[15] especially when different operational protocols are to be combined in a unified platform.[16]

Reliability and robustness are still great challenges of DMF-based micro-reactors[9–14] due to the co-existence of different sorts of chemical reagents and biological species. It is particularly true for those containing sticky constituents, and the various irregular sample-originated surface damages, adsorption, and aging effects[17] of the insulation and hydrophobic materials of the DMF chip. For instance, in a sequential reaction, a droplet sample may fail to reach the expected destination due to a premature charging time, halting the entire system. To address this issue, Shih *et al.*[18] have developed a feedback-control system for DMF, which compares the voltage feedback signal with a threshold voltage to determine whether the droplet has been successfully manipulated to the target electrode before moving to other. However, its sensory unit is fixed to detect only one kind of reagent, being incapable of concurrent execution of a number of droplets with different chemical compositions which frequently occur in many applications. On the other hand, when a movement failure was detected in such a system,[18] a fixed electrode's charging time was added, which can be unnecessarily long. An excessive charging time imposes stress into the dielectric and hydrophobic layers of the DMF chip, aging their performances and reducing their lifetimes.

[a]*State-Key Laboratory of Analog and Mixed-Signal VLSI and FST-ECE, University of Macau, Avenida Padre Tomás Pereira, Taipa, Macao, China.*
E-mail: rmartins@umac.mo
[b]*The Research Centre of Lab on a Chip, Dalian Institute of Chemical Physics, Chinese Academy of Sciences, Dalian, 457 Zhongshan Road, Dalian, China.*
E-mail: bclin@dicp.ac.cn
[c]*On leave from Instituto Superior Técnico, Technical University of Lisbon, Portugal*

† Electronic supplementary information (ESI) available: (1) A text file describing chip fabrication, assembly and operation. (2) Three videos demonstrating multi-droplet manipulation. See DOI: 10.1039/c2lc41156c

‡ Authors who made equal contributions.

Besides, the operation of multiple droplets was restricted to independent actuation of each[19–21] or to the implementation of a synchronous procedure.[22] These may cause deviations from the scheduled itinerary in complex multi-step applications like high-throughput drug screening[23] and cell sorting.[24] Plus, it may result in serious mismanagement and human error when complicated tasks are involved. In view of this, it is highly desirable to establish a real-time position-dependent maneuver mode to avoid manual tuning, and a self-directed expert control to guide multi-droplet manipulation.

This paper describes the first modular DMF system with built-in electronic-control software-defined intelligence. When compared with previous work[25] this design has improved and advanced the control system by introducing fuzzy control and expert control theories, which have been well-established in the electronics' domain.[26,27] They substantiate the advantages of disciplined droplet management and the high efficiency of guiding thorny operation protocols in real time, including: (*i*) the identification of deteriorated electrodes to enhance fault-tolerant behavior; (*ii*) the flexible adjustment of electrode charging time according to droplet hydrodynamics and the aging condition of the dielectric and hydrophobic materials; (*iii*) the interference-free multi-droplet reactions, and (*iv*) the determination of optimum routes for throughput optimization. The three advances are outlined as follows:

The first is the rigid profiling of droplet hydrodynamics. Inspired by the droplet-sensing concept[28] this work managed to experimentally determine the droplet-derived capacitance in real time to serve as the indicator of both static and dynamic droplet positions, which can be easily converted into a digital electrical signal for direct processing in the computer. In other words, all droplets can be tracked without human observation, pre-calibration, visual setup or heavy image signal processing.

The second is fuzzy-based adaptability. We introduce a fuzzy-embodied software engine to compute the optimum electrode charging time and track down the real-time progression of each droplet independent of its chemical composition, securing every manipulation while enhancing both the throughput and lifetime of the DMF chip. Additionally, along such a process, the deteriorated electrodes due to material wear-out can be identified, and renounced instantly by rerouting the droplet pathway.

The third is expert controllability. Rules of droplet routing[29–31] launched by experienced DMF operators can lead to the compilation of a software-defined expert controller with high upgradability to suit different operation protocols. Furthermore, the utilization of a countermeasure decision can logically link up all droplets in real time. As a result, even though there is a wide variety of droplets in asynchronous reactions, droplet-to-droplet or task-to-task interference can still be prevented.

This work should be valuable for scientists and engineers who engage in the standardization and commercialization of more reliable, longer lifetime and user-friendly DMF systems for high-throughput and automated analysis applications.

2 Methods

Details of device fabrication and assembly can be found in the ESI† text and Fig. S1 .

2.1 Architecture and principles of operation of the intelligent DMF system

Our intelligent DMF system (Fig. 1 and ESI†) consists of three subsystems: (*i*) the DMF module (Fig. 1a, Fig. S2 and ESI† text), (*ii*) the DMF chip (Fig. 1b and ESI†), and (*iii*) the operation unit (Fig. 1c and ESI†). First, the DMF chip with droplets is mounted on the chip holder. Second, each droplet is identified and located. Finally, the operation unit generates the droplet routing plan and actuates the droplet using the EWOD force in real time.

The operation unit is based on a real-time feedback positioning mechanism. The embedded protocol can precisely track the static or dynamic position of each droplet, being capable to drive complex droplet transportation. The DMF chip is patterned with a 4 × 6 electrode matrix (Fig. 1b), which is connected to the control electronics (Fig. 1d) to meet multi-droplet non-invasive routing plans. Also, the feedback-based fuzzy-enhanced control theory (Fig. 1e) is embodied into the system to correct the droplet transporting error (*e.g.*, a droplet cannot cover the target electrode perfectly), ensuring the fidelity of each droplet transportation.

The DMF chip consists of 24 independent electrodes that are driven by the control electronics (Fig. 1a, the mid layer) to switch between the voltage-actuation mode (7 to 15 V_{rms} were used in this work) and the droplet-sensing mode. For the latter, the field programmable gate array (FPGA, Fig. 1a, the bottom layer) scans the capacitance of each electrode using an oscillator outputting variable-frequency pulses. The collected frequency information is transferred to the operation unit (*i.e.*, the computer) for real-time computation, and finally fedback to the DMF chip.

2.2 Fuzzy-control for droplet-position correction

2.2.1 Volume measurement. The distinction between the capacitance values of water and surrounding medium (*e.g.*, air or silicon oil) has been utilized for droplet-volume measurements.[28,32] The parallel-plate structure of a DMF chip behaves electrically as a capacitor, thus allowing capacitance-derived droplet-volume measurement. Inspired by this, our experimental setup can be found in Fig. 2a. The device was designed to test the response of our sensing module to the volume growth of a droplet on a tailored electrode. DI water, phosphate buffered saline (PBS) and 1% bovine serum albumin (BSA) in PBS were injected from the top of a DMF electrode (4 × 11 mm) *via* a hole with a constant flow rate of 5 μL min^{-1} by a syringe pump, from which the droplet volume can be determined with respect to the pumping time. The droplet connects the oscillator circuit *via* a tailor-made electrode in series. The change of impedance, mainly due to the capacitance variation,[32] is inversely proportional to the output oscillation frequency collected from the droplets.

2.2.2 Location measurement. In droplet positioning, the centre of the electrode is the target which the droplet should reach for. In practice, during most of our experiments, the

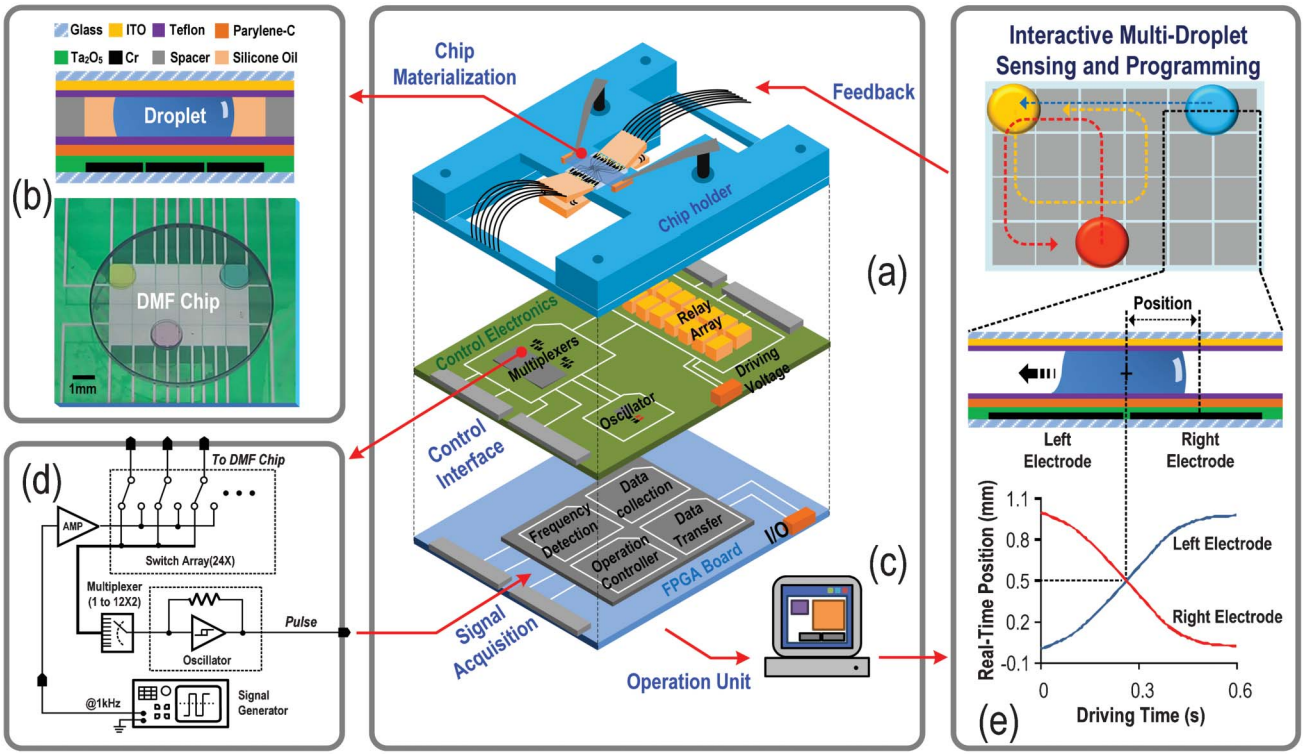

Fig. 1 Proposed control-engaged digital microfluidic (DMF) technology. (a) The DMF module is composed of three operation layers. The top layer is an ergonomically designed chip holder that allows user-friendly operation and experimental repeatability. The mid layer is the control electronics which fits the size of the testbench. The bottom layer is the field-programmable gate array (FPGA) board. (b) The fabricated DMF chip features optimized materialization to enhance the speed-to-voltage efficiency of droplet manipulation using the electrowetting-on-dielectric (EWOD) behavior. (c) The operation unit powered by the inference mechanism in the computer is capable to perform (*i*) feedback-based position correcting, (*ii*) fuzzy-enhanced droplets control, and (*iii*) droplet transportation sequence programming. (d) The control electronics performing real-time multi-droplet actuation and sensing. The presence/absence of droplet in each electrode is converted into clocked pulses *via* multiplexing each electrode to a single oscillator. (e) The operation unit features a user-friendly and upgradable human-control interface to manage the entire module.

initial placement of each droplet on the DMF chip will drift due to possible human error, or due to an inconsistent space difference between the top (ITO glass) and bottom (DMF chip) plates that induces a surface-tension difference, thus undesirably moving the droplets. Thus, an ideal DMF system should be able to position each droplet automatically before any operation. By scanning the capacitance of each electrode, the capacitances of every two adjacent electrodes to the ground can be obtained as C_i and C_t (Fig. 2b). Equipped with the volume measurement means as above, it is practical to

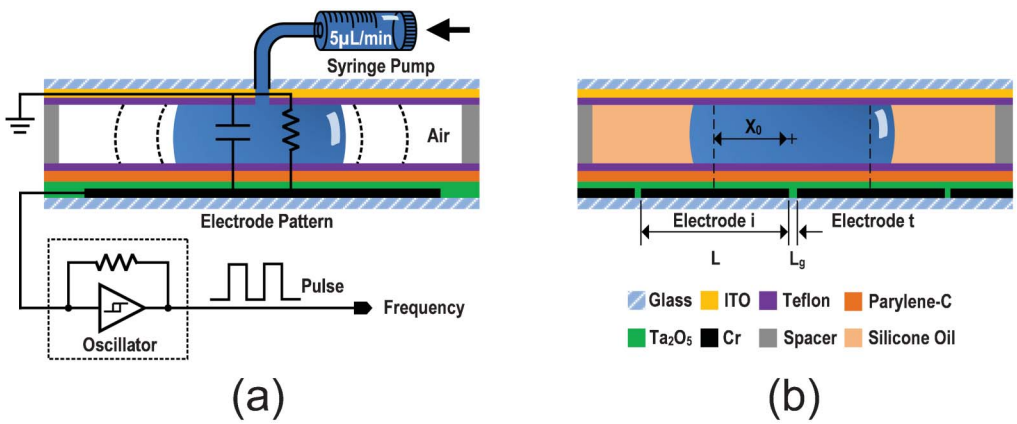

Fig. 2 (a) Capacitance measurement module. Real-time measurement of liquid volume of a droplet *versus* the oscillator output frequency. (b) Droplet positioning between two adjacent electrodes.

estimate the surface coverage of a droplet from one electrode to its adjacent by comparing the capacitance between them, according to the droplet-location estimating equation:[28]

$$X_0 \cong \frac{C_t}{(C_i + C_t)}(L + L_g) \quad (1)$$

where X_0 is the dynamic position between two adjacent electrodes, L is the electrode pitch length and L_g is the gap between electrodes. Since L_g (10 μm) is much smaller than L (1 mm), eqn (1) can be simplified as:

$$X_0 \cong \frac{C_t}{(C_i + C_t)} \quad (2)$$

which is a droplet-independent ratio-based parameter, ideal as the threshold value to evaluate the success of liquid movement. The suitable X_0, as the threshold value R_{thresh}, should be under 100% completion of the droplet transportation. The "% completion" parameter is defined as the number of successful droplet movements divided by the total number of programmed steps. Apparently, as the initial input in our system is a digital signal featuring a capacitance-derived clock frequency for position estimation by the computer, it is much more compatible with an electronic controller than other visual images[33] of a moving droplet for on-line control purposes.

2.2.3 Reference charging time. The voltage-dependent maximum rate at which droplets could be transferred between three adjacent electrodes was determined by actuating a 1 kHz AC voltage signal (7 to 15 V_{rms}). Meanwhile, the relationship between droplet position and charging time could be *in situ* obtained by our droplet positioning system above, based on which displacement percentages of the leading edges of the droplet with respect to their previous positions were calculated. The maximum velocity (V_{max}) was then given by: $L \times$ maximum displacement percentage/charging time, where L is the electrode pitch. The measurement was obtained three times with high repeatability at each point. As a result, a reference charging time T_{ref} can be determined as:

$$T_{\text{ref}} = L/V_{max} \quad (3)$$

2.2.4 Fuzzy control. The principle of fuzzy-enhanced droplet movement control is illustrated in Fig. 3a. The range of input V_x was defined from 0 to 40 V. Five triangle membership functions were defined in the voltage fuzzy sets, namely: very low, low, medium, high and very high. The range of input D_x was defined from 0 to 1 mm. Five Gaussian membership functions were defined in position fuzzy sets, namely: very far, far, medium, close and very close. The range of output G_f was defined from 0 to 200%. Twenty-five triangle membership functions were defined in G_f fuzzy sets. The names of these membership functions were related to their output intensity. A fuzzy inference engine was built in MATLAB®, Fuzzy inference system (FIS). Fuzzy rule base and fuzzy inference function methods are showed in the ESI† (Tables 1 and 2). The working principles can be described as follows: Firstly, a reference electrode's charge time (T_{ref}) derived from eqn (3)

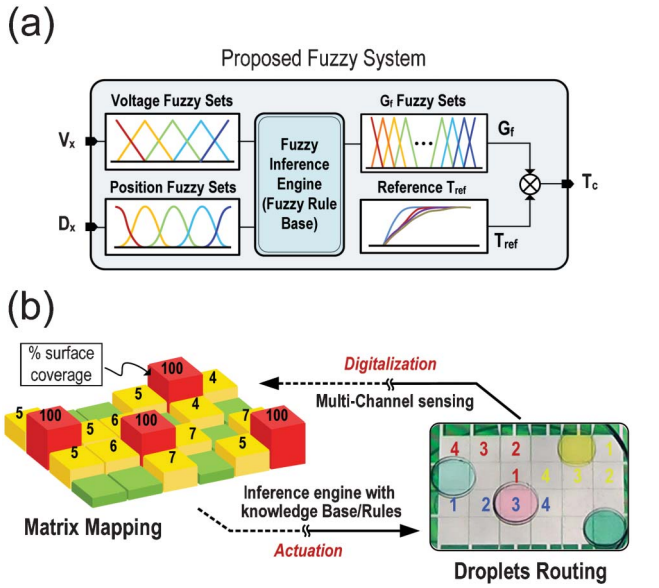

Fig. 3 (a) Fuzzy-enhanced control for droplet-position correction operation principle. (b) The close-loop process for multi-droplet routing. Multi-channel sensing is to digitalize the droplet on DMF chip, and a corresponding matrix mapping will be generated by the operation unit. Afterwards, the droplet routing plan which is created by the inference engine with knowledge and rules will be actuated to the corresponding electrodes.

will be applied to the target electrode for each transportation step to get a responding dynamic position (D_x) of the involved electrodes. Secondly, the dynamic position and the corresponding effect value of driving voltage (V_x) will be fuzzified by their fuzzy sets. Thirdly, the acquired fuzzified inputs will be evaluated with the inference mechanism powered by the fuzzy inference engine (built in MATLAB® and called by the design software in real time). Finally, the obtained result will be defuzzified by G_f fuzzy sets into the coefficient factor of compensation charging time, G_f. Thus, the fuzzy-enhanced electrode's compensation charge time (T_c) is given by:

$$T_c = T_{\text{ref}} \times G_f \quad (4)$$

In fact, T_c can also be applied to the droplet more than once, *i.e.*:

$$T_{c,n} = (T_{\text{ref}} + T_{c1} + T_{c2} + \ldots + T_{c,(n-1)}) \times G_{f,n} \quad (5)$$

until the droplet movement is complete. In our experiments, DI water was programmed to be transported over five electrodes. The total charging time T_{total} of the five steps is:

$$T_{\text{total}} = \Sigma_{n=1}^{5} T_{\text{step},n} \quad (6)$$

In case of bare feedback system, the total time $T_{\text{step,bare}}$ would be:

$$T_{\text{step,bare}} = n \times T_{\text{ref}} \quad (7)$$

where n is the number of charging times. On the other hand, the time taken in each step by the proposed fuzzy-enhanced feedback-control system is given by:

$$T_{\text{step,fuzzy}} = T_{\text{ref}} + \Sigma_1^n T_{c,n} \quad (8)$$

where $T_{c,n}$ is obtained from eqn (4).

2.3 Expert control for multi-droplet management

As shown in Fig. 3b an expert controller was designed to enhance the multi-droplet manageability. Assisted by the multi-channel sensing circuit that offers real-time tracking of droplet location, the controller checked with the rules which were previously collected from experienced DMF operators (stored in the course rule source in the knowledge base), and supervised the routing of the droplets by determining the sequence of the related relay switch with the inference engine. To define the basic rules, the coordinates of the electrodes which were occupied by droplets are labeled and classified as follows: (*i*) the static mode uses (A_x, A_y) or (B_x, B_y), in which a droplet is in a stationary manner; (*ii*) the active mode uses ($^*A_x$, $^*A_y$) or ($^*B_x$, $^*B_y$), in which a droplet is in motion; (*iii*) the breakdown mode uses (Z_x, Z_y) which indicates that an electrode has been broken down. Under the basic rules, the distances between the droplets are classified, depending on their status and positions to avoid unwanted merging or faults. The details of the anti-merging or faults rules can be illustrated as follows: for droplet A, if,

$$|Z_x - A_x| < 1 \text{ or } |Z_y - A_y| < 1 \quad (9)$$

droplet A will steer clear of the breakdown electrode;

$$|A_x - B_x| < 2 \text{ or } |A_y - B_y| < 2 \quad (10)$$

droplet A will step aside from the static droplet B;

$$|A_x - {}^*B_x| < 3 \text{ or } |A_y - {}^*B_y| < 3 \quad (11)$$

$$|{}^*A_x - {}^*B_x| < 3 \text{ or } |{}^*A_y - {}^*B_y| < 3 \quad (12)$$

droplet A will back off from the moving droplet B.

3 Results and discussion

3.1 Real-time volume measurement

As shown in Fig. 4a, the relationship between the inverse of frequency and droplet volume of three kinds of chemical reagents with a high resolution, namely DI water, PBS and PBS with 1% BSA are illustrated. All these plots demonstrated an excellent linearity with R^2 greater than 0.999. These results validate the droplet-volume quantification on the detected electrode. Besides, the similar slopes of these three reagents indicate the capability of detecting different kinds of reagent, simultaneously, by our capacitance-based feedback mechanism. However, pre-calibration may be necessary for very different liquids.

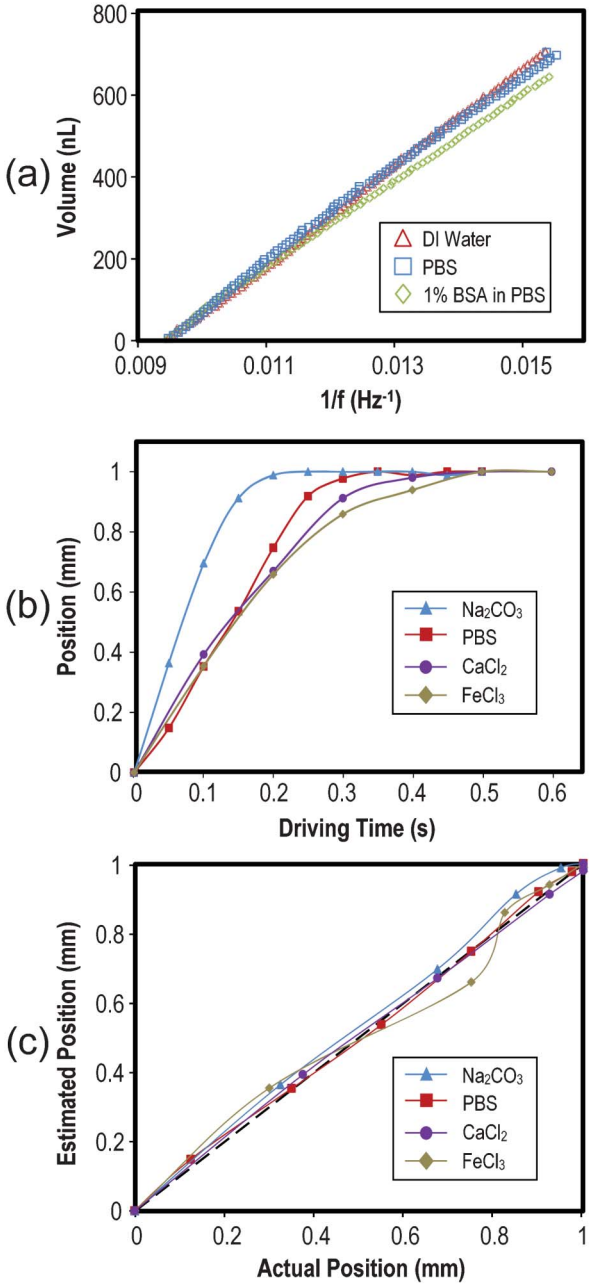

Fig. 4 (a) Inversion of frequency measured by oscillator circuit *vs.* droplet volume. Excellent linear relationship and calibration were obtained. The relationship was verified under a number of liquids: distilled (DI) water, PBS and BSA. (b) The tracks of PBS, Na_2CO_3, $FeCl_3$ and $CaCl_2$ droplets across an energized electrode. (c) Actual and estimated droplet position plot from experiments.

3.2 Complexity of a DMF droplet actuator

During each step of droplet movement from one electrode to its neighbor (1 mm), a continuous state of actuation occurs. It was found that the EWOD force-induced displacement of a droplet *versus* the transport time exhibits a nonlinear relationship. Also, as illustrated in Fig. 4b and video 1 (ESI†), the alterations of the position of the droplets with electrolytes during this state are distinct of each other even though it was found that those droplets with the same contents are faithfully

repeatable. In the experiments, the moving velocities for droplets containing 0.1 mol L^{-1} Na_2CO_3, PBS, $CaCl_2$ and $FeCl_3$ to travel from the initial electrode to the end of the target electrode, were 5 mm s^{-1}, 2.85 mm s^{-1}, 2.5 mm s^{-1} and 2 mm s^{-1}, respectively. These profiles of electrolyte, which are frequently used in micro-reactors, revealed that the difference in the contents of the droplets also leads to different optimum charging times, due to their dissimilar viscosities.[34] The movement of 0.1% BSA in PBS, which is normally used in microfluidic communities because it adheres firmly to DMF hydrophobic surfaces,[35] was also observed with a velocity of 0.88 mm s^{-1} under a low actuation voltage of 15 V_{rms}. Regarding the slow movement of BSA, it was found that biofouls occurred and delayed the transportation of the droplet, which can be alleviated by adding surfactant[35] or increasing the driving voltage. Fig. 4c compares the actual and capacitive droplet position estimated from the experiments for different liquids. The visual droplet position was measured from the top-view images taken by camera (the camera scale was calibrated by the size of the electrode). The droplet position was estimated using eqn (2). When compared with the previous report,[28] a more accurate tracking scheme with smaller error (<18%) was achieved in our work. Different behaviors in the movement of chemical and biological samples complicate the setup of the DMF charging time for applications with various interactions. The establishment of the quantitative hydrodynamic profiles, confirmed by our experiments, serves as the core rationale for setting up a fuzzy-enhanced control protocol to be described later.

Besides, with the proposed feedback-based droplet positioning, the droplet can be precisely located or relocated to the targeted positions automatically. Thus, even if there is a strong wear-out of the ITO glass and DMF chip after a long operation period, the feedback mechanism can update the basic capacitance of each electrode into the database, being rather immune to the change of the environmental conditions.

3.3 Fuzzy control for droplet-position correction

Several practical uncertainties can affect the robustness and repeatability of DMF-based systems. Examples are: (*i*) the thickness of the insulation and hydrophobic layers on individual DMF chips; (*ii*) the size and contents of different reagent droplets, and (*iii*) the magnitude, frequency and pulse duration of the charging voltage. All of these can lead to a deviated droplet transport distance under the EWOD force. In this work, the charging time was chosen as the compensation parameter that can be automatically adjusted by the control coordinating program to correct the performance variation. On the other hand, when a droplet moves from one electrode to the next, the velocity varies with each transient position. Specifically, the velocity of the droplet decays when it gets closer to the target electrode. Thus, a tailored fuzzy-control system optimizing the electrode's charging time is proposed to enhance both the throughput and fidelity of droplet transportation.

To validate the proposed fuzzy-enhanced droplet movement control algorithm for multi-droplet manipulation, the % completion of different reagents without extra calibration (the threshold value R_{thresh} was set to 0.75) has been studied. It was found that the DI water, PBS and 0.1% BSA in PBS can be transported with 100% completion. As shown in Table 1, to find an optimum R_{thresh}, eight trials from 0.55 to 0.9 were tested with different kinds of liquid (*i.e.* DI water, PBS and 0.1% BSA in PBS). In a 5-step movement with 10 trials, 100% completion can be achieved when R_{thresh} ranges from 0.75 to 0.8, with an average velocity of 1.85 mm s^{-1}, 1.51 mm s^{-1} and 0.88 mm s^{-1} for DI water, PBS and 0.1% BSA in PBS, respectively. Indeed, 0.75 to 0.8 R_{thresh} are all robust, proving that the proposed DMF system can effectively manage multi-droplet manipulation without extra calibration that was required in the prior art.[18] In Table 1, when the R_{thresh} value was set as 0.9, which was always larger than the real-time calculated position, the feedback system suffered from a dead cycle, thus only 1 successful step out of 5 (20%) was achieved.

Another experiment is to study the relationship between the charging time and T_{ref} to find the optimum droplet movement velocity. A droplet is set to run over five successive electrodes. At a driving voltage of 7 V and with five different T_{ref} values from 0.1 to 0.5 s, a comparison of overall charging duration between the bare feedback-control and fuzzy-enhanced feedback-control corrections was made. Fig. 5a shows the derived defuzzification scheme of G_f. According to Fig. 5b, the fuzzy-enhanced feedback-control saves up to 21% charging time. From our experiments, we observed that the optimum charging time is when the ratio between T_{ref} to the average charging time of each step is around 40%. This observation should be highly relevant for droplet management, since plenty of varieties might exist in such a complex system, as already mentioned.

3.4 Expert control for multi-droplet management

An example (video 2†), in which the logic links between two droplets (both set to active mode) were built, is presented to illustrate how the basic anti-merging rules work in the proposed expert controller. A red droplet was coordinated to require the fewest number of steps to shunt away from the non-invasive region of the blue droplet with the anti-merging/fault rules. This dual-droplet non-invasive transportation demo shows the basic principle of countermeasure decision for effective management of multiple droplets on a DMF chip.

Another example, in which logic links between four droplets were established, is presented also to show how the expert controller handles more complex situations. As shown in Fig. 6 and video 3†, the red and blue droplets are programmed for

Table 1 Transport of liquids with different threshold values

	Average %completion		
R_{thresh}	DI Water	PBS	0.1% BSA in PBS
0.9	20%	20%	20%
0.85	100%	64%	100%
0.8	100%	100%	100%
0.75	100%	100%	100%
0.7	100%	100%	98%
0.65	84%	98%	76%
0.6	52%	70%	73%
0.55	22%	56%	20%

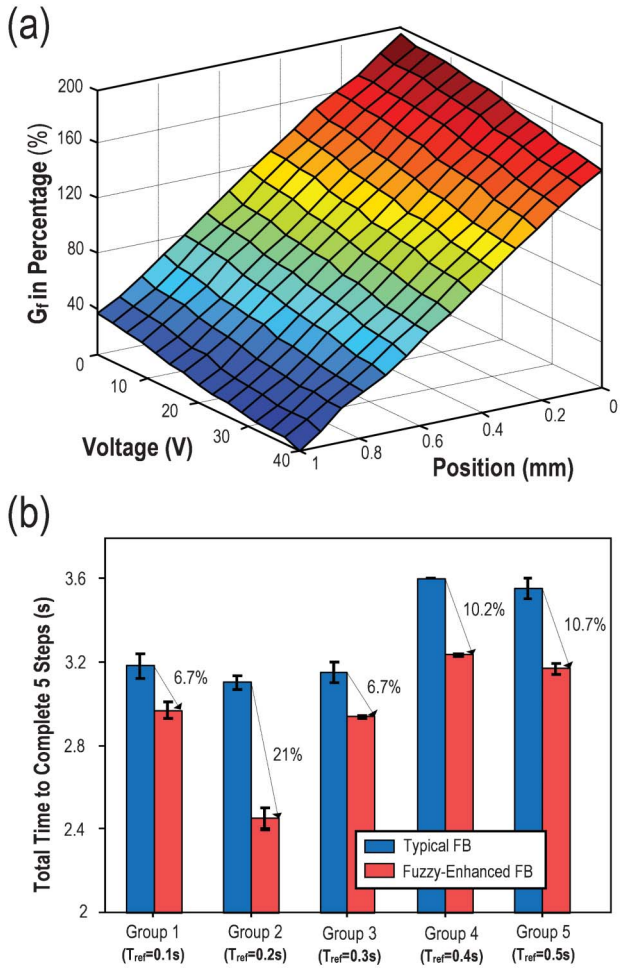

Fig. 5 (a) Defuzzification scheme of G_f, with the output expressed as a percentage of the reference charging time, T_{ref}. (b) A comparison between the two algorithms of feedback control (typical and fuzzy-enhanced) of the total charging time for a droplet to complete the movement across five consecutive electrodes. Each experiment was repeated ten times, and error bars are ± 1 SD.

continuous circulation before they are caught (yellow and cyan droplets are preset in a static mode). A yellow droplet tried to capture a circulating blue droplet while a red droplet also kept travelling in a square course. In the meantime, a cyan droplet stayed at the lower right corner of the chip to act as a stationary barrier. Under these circumstances, in addition to the basic rules, others were hierarchically updated in the knowledge database of the expert controller and assisted the control coordinator in the decision making process of the droplet-capture demonstration: (*i*) the distance between the blue and yellow droplets keeps shrinking as the droplet moves, and (*ii*) on the course where the yellow droplet runs, if the red droplet is about to hinder it, then the basic anti-merging/fault rule overrules rule (*i*) to impose the yellow droplet to change its course and revert to a safe place. As a result, the yellow droplet successfully captured the blue without being intercepted by the red. This example partially demonstrated the intelligence of the proposed controller: (*i*) under any circumstance, the control coordinator senses the instantaneous position change of the droplet, checks and takes a countermeasure decision on the necessary routes and the fewest steps possible, which are implemented *via* the inference engine; (*ii*) in any instant, the action taken by the blue droplet depends on the position and the status of the other droplets. An event-driven logic control of droplet position was implemented here. Also, in video 3†, the fourth droplet in cyan capturing the formerly-chasing red droplet further demonstrated the performance of the event logic control mode. The second chase and capture and the final merging between the two larger droplets was initiated upon the event of the first merge, rather than under a pre-fixed timed order. Both of the two examples demonstrated the advantages of flexibility and accuracy over a sequence logic control process. This proves the feasibility of the technique in serial reactions, and (*iii*) the database in the expert controller can be easily updated and adapted to specific applications. When compared with the conventional automatic control mode, the proposed expert controller exhibits learning ability and a coherent order of rules. For example, a prolonged lifetime and improved reliability of a DMF chip can be obtained if a record of the frequently-used and prone-to-breakdown individual electrodes is filed and renewed in the proposed routing coordinator, for droplets to circumvent during the continuous operation of the DMF system.

4 Conclusions

Firstly, the different hydrodynamic behaviors of droplets with different contents in their dynamic state were explored by monitoring the real-time capacitance change on each electrode, and any dissimilarities were attributed to the difference in their surface charge densities and viscosities. With the displacement profiles recorded, it was inferred that a pre-fixed electrode charging time and the lack of an appropriate controller may cause misconduct of droplet routing in DMF-based micro-reactors. Secondly, an intelligent-control DMF system was proposed to address the complicated hydrodynamic problems: (*i*) during the dynamic process of a droplet, an optimized charging time which was set by the fuzzy controller avoids overdriving the electrodes. In this process, the definition of a short empirical reference time is favorable; (*ii*) in the case of multiple-droplet routing, novelties were verified in the proposed expert multi-droplet controller. Characteristics such as countermeasure decision and event logic control for droplet routing, hierarchy of rules and learning ability of the controller were also integrated in the design. Finally, a new expert controller allows autonomous management of the droplet routing, disturbance and fault-tolerance operation of the DMF chip.

We believe that the involvement of an electronic-based fuzzy-feedback control in a DMF-based droplet platform will equip it with adequate intelligence to manage a larger number of dissimilar droplets in large-scale micro-reactors. As this work is the first prototype, we believe the cost can be significantly reduced upon proper circuit-level and board-level optimization such as using low-cost ASIC integrated circuits to

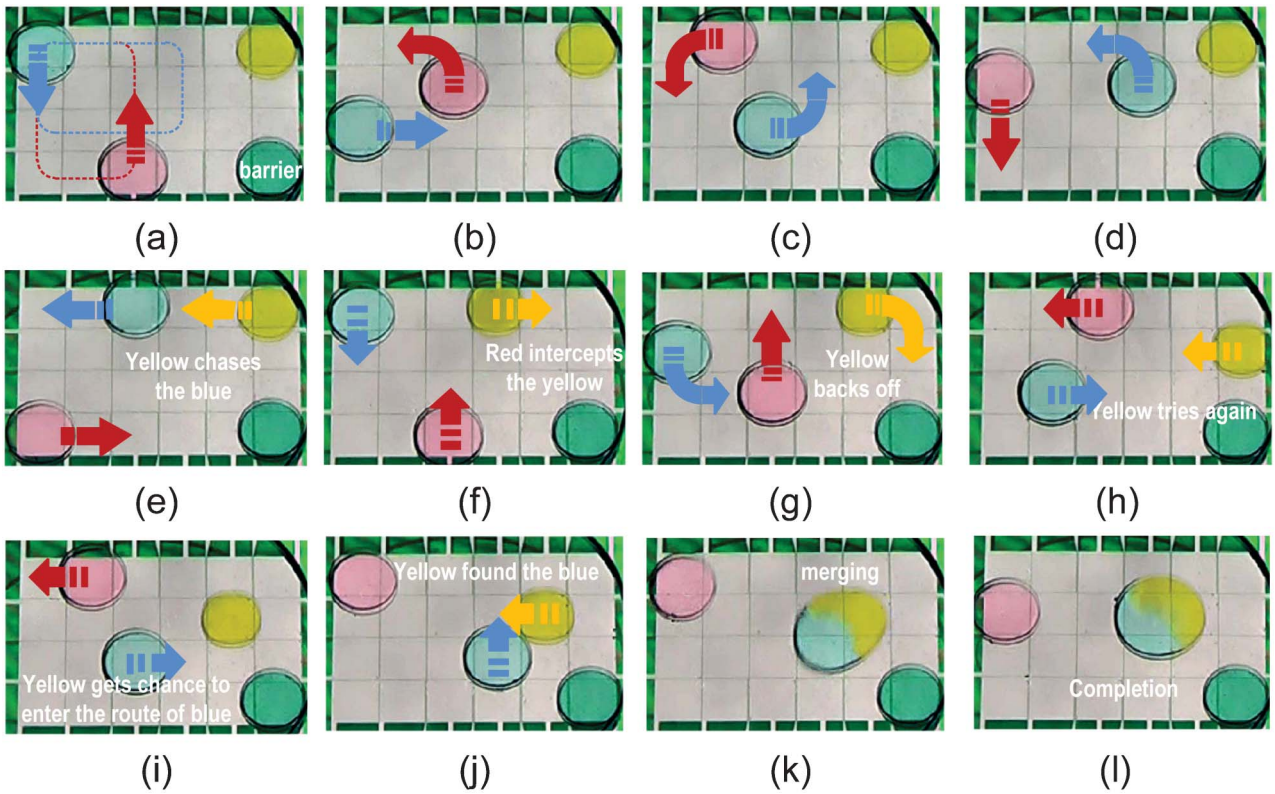

Fig. 6 Expert controller-based 4 droplet routing (movie†). (a–d) The red and blue droplets are programed for continuous circulation (2 s frame^{-1}). (e–h) The yellow droplet is ordered to chase the blue, but backs-off when disturbed by the red (1 s frame^{-1}). (i–l) The yellow droplet chases the blue, successfully, when the red droplet is peripheral (0.5 s frame^{-1}).

replace the switches and FPGA. Thus, it is expected that this research should be highly valuable for scientists and engineers who work on the standardization and commercialization of a more reliable, reconfigurable and longer lifetime control-engaged DMF system for automated analysis, or as the control platform of high-throughput multi-droplet reaction applications.

Acknowledgements

We thank Chi-Pang Lam for his initiation on the system set-up; Cheng Dong for his discussion and collaboration on the software design; Pengju Cao and Junxuan Luo, from the University of Shenzhen, and Long Sun from DICP-CAS for their technical support on Ta_2O_5 fabrication and characterization; Can Li from DICP-CAS for his help in metallization; Jason Hsu and Lee Lung-chih from La Chi Enterprise, for their discussion on parylene C coating; and Rentao Zhong for the volume measurement set-up. This work was supported by the Research Committee of the University of Macau and Macao Science and Technology Development Fund (FDCT, No. 033/2011/A2), Macao, and the National Natural Science Foundation of China (NNSFC, No. 21176232).

References

1 A. R. Wheeler, *Science*, 2008, **322**, 539–540.
2 R. B. Fair, *Microfluid. Nanofluid.*, 2007, **3**, 245–281.
3 R. B. Fair, A. Khlystov, T. D. Tailor, V. Ivanov, R. D. Evans, P. B. Griffin, V. Srinivasan, V. K. Pamula, M. G. Pollack and J. Zhou, *IEEE Des. Test Comput.*, 2007, **24**, 10–24.
4 P. Y. Keng, S. Chen, H. Ding, S. Sadeghi, G. J. Shah, A. Dooraghi, M. E. Phelps, N. Satyamurthy, A. F. Chatziioannou, C. J. Kim and R. M. V. Dam, *Proc. Natl. Acad. Sci. U. S. A.*, 2012, **109**, 690–695.
5 M. J. Jebrail and A. R. Wheeler, *Anal. Chem.*, 2009, **81**, 330–335.
6 R. S. Sista, A. E. Eckhardt, V. Srinivasan, M. G. Pollack, S. Palanki and V. K. Pamula, *Lab Chip*, 2008, **8**, 2188–2196.
7 E. M. Miller and A. R. Wheeler, *Anal. Chem.*, 2008, **80**, 1614–1619.
8 V. Srinivasan, V. K. Pamula and R. B. Fair, *Lab Chip*, 2004, **4**, 310–315.
9 L. Malic, T. Veres and M. Tabrizian, *Biosens. Bioelectron.*, 2009, **24**, 2218–2224.
10 S. H. Yoon, J. Chang, L. Lin and M. R. K. Mofrad, *Lab Chip*, 2011, **11**, 3555–3562.
11 S. Srigunapalan, I. A. Eydelnant, C. A. Simmons and A. R. Wheeler, *Lab Chip*, 2012, **12**, 369–375.
12 S. K. Fan, H. Yang and W. Hsu, *Lab Chip*, 2011, **11**, 343–347.

13 D. Chatterjee, B. Hetayothin, A. R. Wheeler, D. J. King and R. L. Garrell, *Lab Chip*, 2006, **6**, 199–206.
14 S. Millefiorini, A. H. Tkaczyk, R. Sedev, J. Efthimiadis and J. Ralston, *J. Am. Chem. Soc.*, 2006, **128**, 3098–3101.
15 K. Goda, A. Ayazi, D. R. Gossett, J. Sadasivam, C. K. Lonappan, E. Sollier, A. M. Fard, S. C. Hur, J. Adam, C. Murray, C. Wang, N. Brackbill, D. D. Carlo and B. Jalali, *Proc. Natl. Acad. Sci. U. S. A.*, 2012, **109**, 11630–11635.
16 M. G. Pollack, A. D. Shenderov and R. B. Fair, *Lab Chip*, 2002, **2**, 96–101.
17 L. Malic, D. Brassard, T. Veres and M. Tabrizian, *Lab Chip*, 2010, **10**, 418–431.
18 S. C. C. Shih, R. Fobel, P. Kumar and A. R. Wheeler, *Lab Chip*, 2011, **11**, 535–540.
19 L. Luo and S. Akella, *Proceedings of the 2007 IEEE/RSJ International Conference on Intelligent Robots and Systems*, San Diego, CA, USA, Oct 29–Nov 2, 2007, 3151–3157.
20 K. F. Böhringer, *IEEE Transactions on CAD of Integrated Circuits and Systems*, No.2, Feb. 2006, **vol. 25**, pp. 329–339.
21 Z. Hua, J. L. Rouse, A. E. Eckhardt, V. Srinivasan, V. K. Pamula, W. A. Schell, J. L. Benton, T. G. Mitchell and M. G. Pollack, *Anal. Chem.*, 2010, **82**, 2310–2316.
22 M. J. Jebrail, H. C. Ng, V. Rai, R. Hili, A. K. Yudin and A. R. Wheeler, *Angew. Chem., Int. Ed.*, 2010, **49**, 8625–8629.
23 P. B. Gupta, T. T. Onder, G. Jiang, K. Tao, C. Kuperwasser, R. A. Weinberg and E. S. Lander, *Cell*, 2009, **138**, 645–659.
24 J. C. Baret, O. J. Miller, V. Taly, M. Ryckelynck, A. E. Harrak, L. Frenz, C. Rick, M. L. Samuels, J. B. Hutchison, J. J. Agresti, D. R. Link, D. A. Weitz and A. D. Griffiths, *Lab Chip*, 2009, **9**, 1850–1858.
25 T. Thorsen, S. J. Maerkl and S. R. Quake, *Science*, 2002, **298**, 580–584.
26 K. S. Fu, *IEEE Trans. Autom. Control*, 1971, **16**, 70–72.
27 S. J. Huang and W. C. Lin, *Journal of Vibration and Control*, 2003, **9**, 1023–1040.
28 M. A. Murran and H. Najjaran, *Lab Chip*, 2012, **12**, 2053–2059.
29 K. Chakrabarty, R. B. Fair and J. Zeng, *IEEE Trans. Comput.-Aided Des. Integr. Circuits Syst.*, 2010, **29**, 1001–1017.
30 Z. Chen, D. Teng, G. Wang and S. Fan, *BioChip J.*, 2011, **5**, 343–352.
31 P. Roy, H. Rahaman and P. Dasgupta, *Integration*, 2012, **45**, 316–330.
32 J. Gong and C. J. Kim, *Lab Chip*, 2008, **8**, 898–906.
33 R. Baviere, J. Boutet and Y. Fouillet, *Microfluid. Nanofluid.*, 2008, **4**, 287–294.
34 V. Bahadur and S. V. Garimella, *J. Micromech. Microeng.*, 2006, **16**, 1494–1503.
35 V. N. Luk, G. C. Mo and A. R. Wheeler, *Langmuir*, 2008, **24**, 6382–6389.